Liquid Crystals
Publication details, including instructions for authors and subscription information:
http://www.informaworld.com/smpp/title~content=t713926090

Electric field-induced birefringence, optical rotatory power and conoscopic measurements of a chiral antiferroelectric smectic liquid crystal

V. Manjuladevi[a]; J. K. Vij[a]
[a] Department of Electronic and Electrical Engineering, Trinity College Dublin, University of Dublin, Dublin 2, Ireland

To cite this Article Manjuladevi, V. and Vij, J. K.(2007) 'Electric field-induced birefringence, optical rotatory power and conoscopic measurements of a chiral antiferroelectric smectic liquid crystal', Liquid Crystals, 34: 8, 963 — 973
To link to this Article: DOI: 10.1080/02678290701478103
URL: http://dx.doi.org/10.1080/02678290701478103

Liquid Crystals, Vol. 34, No. 8, August 2007, 963–973

Taylor & Francis
Taylor & Francis Group

Electric field-induced birefringence, optical rotatory power and conoscopic measurements of a chiral antiferroelectric smectic liquid crystal

V. MANJULADEVI and J. K. VIJ*

Department of Electronic and Electrical Engineering, Trinity College Dublin, University of Dublin, Dublin 2, Ireland

(*Received 12 March 2007; accepted 26 April 2007*)

Using a photoelastic modulator-based novel set-up, the electric field-induced in-plane birefringence and the optical rotatory power (ORP) were measured of an antiferroelectric liquid crystalline compound (12OF1M7) in its various phases using 30 μm homeotropic cells. Some specific signatures of the in-plane birefringence and of the ORP for the various phases are being established. A relatively small threshold field is needed for the unwinding process of the antiferroelectric phase with a unit cell of four layers [SmC_A*(1/2)] compared with that for two layers [SmC_A*(0)]. On application of the electric field on the high temperature side of the SmC_A*(1/2) phase (80.1–81.5°C), a field-induced phase transition is shown to occur directly to the SmC* phase, whereas on the lower temperature side (79.4–80.1°C) the transition takes place to SmC* via the SmC_A*(1/3) phase. The in-plane birefringence exhibits a critical power law dependence for the SmC*–SmA transition. The ORP changes sign within the temperature range of the phase with a unit cell of three layers, reflecting a change in the handedness during this phase. Using tilted conoscopy, the results for the biaxiality and the apparent tilt angle for a smectic liquid crystal with a tilt angle greater than 18° in the ferroelectric phase are reported. The biaxiality implies the difference in the refractive indices between the two minor axes of the refractive index ellipsoid. The optical transmittance at visible and IR wavelengths for free-standing films reveal characteristic reflection bands for these phases. The modulated structures of the reflected bands appear just above the SmC_A* phase and below SmC_A*(1/3); these are possibly due to an easy deformation of the phase by the surfaces.

1. Introduction

Chiral smectic liquid crystals (LCs) can exhibit several biaxial phases [1–3] with a relatively long helical pitch, the value of which ranges from ~0.4 μm to several μm. The number of layers in a unit cell varies from one to usually four. The synclinic (or SmC*) phase has a unit cell of a single layer [4], whereas the anticlinic (or SmC_A*) has a unit cell of two layers [1]. Since the helical pitch is usually longer than the optical wavelength, the phases in which the molecular directors are tilted from the smectic layer normal are known as biaxial phases. Biaxial phases (subphases) with a unit cell of five and eight layers [5] have also been observed, but these are found to exist in only some chiral compounds and only over a very narrow range of temperatures. In addition, a SmC_α* phase appears in between the SmA and SmC* phases. This is characterized by a very short helical pitch, of the order of ~10 to 50 nm, and a unit cell having a non-integral multiple number of layers [6–8]. Since the helical pitch is much shorter than the visible wavelength, this often is termed as the uniaxial phase on the scale of the optical wavelength. This phase appears only in chiral compounds that are synthesized with usually large optical chiral purity. In the ferroelectric SmC* phase, the molecules are tilted at an angle (θ) with respect to the layer normal. Due to the molecular chirality, the direction of the tilt precesses along the layer normal resulting in a helical structure. It has recently been shown that competition between the forces that give rise to the synclinic and the anticlinic phases leads to a range of the intermediate ferrielectric phases and the polarizations arising from both the chirality and the discrete flexoelectricity play important roles in giving rise to a number of uniaxial and biaxial subphases [9, 10]. Isozaki *et al.* [11] designated these phases as SmC_A*(q_T), where q_T=[F]/([A]+[F]) and [F] and [A] represent the ferroelectric and antiferroelectric orderings. Hence, SmC_γ* phases with a unit cell of three layers and an antiferroelectric phase with a unit cell of four layers are referred to as SmC_A*(1/3) and SmC_A*(1/2) phases, respectively. SmC_A* phase with a

*Corresponding author. Email: jvij@tcd.ie

Liquid Crystals
ISSN 0267-8292 print/ISSN 1366-5855 online © 2007 Taylor & Francis
http://www.tandf.co.uk/journals
DOI: 10.1080/02678290701478103

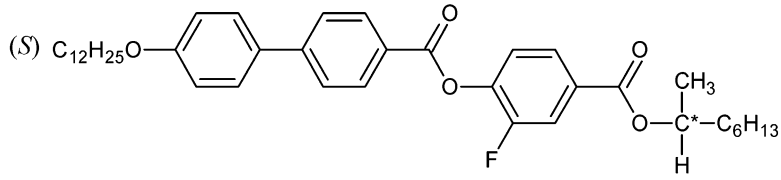

Figure 1. The structural formula of the compound (*S*)-12OF1M7.

unit cell of two layers is simply referred to as SmC_A*(0), since its q_T value is 0.

Conoscopy was initially used by Gorecka *et al.* [12]. not only to characterize ferrielectric and antiferroelectric phases but also for finding the number of layers and the distribution of the azimuthal angles of the in-layer directors in a unit cell. The number of layers in a unit cell determined by conoscopic experiments by Gorecka *et al.* [12] has correctly been confirmed for SmC_A*(0), SmC_A*(1/3) and SmC_A*(1/2) using the sophisticated technique of resonant X-ray scattering by Mach *et al.* [13] However, the distribution of the azimuthal angle of the directors determined through accurate ellipsometeric measurements first determined by Johnson *et al.* [14] was found to depart somewhat from the distributions initially suggested from conoscopic and the electro-optic experiments in terms of the Ising model. Using the conventional conoscopic technique, the exact measurement of the biaxiality of the chiral smectics with a tilt angle larger than $\sim 18^\circ$ was not possible since the centres of the meletopes of the conoscopic image went out of the field of view [12]. We recently developed the technique of tilted conoscopy [15], whereby biaxiality can be measured with a precision of ± 0.0005 for the tilted smectics for a tilt angle up to 45°. Biaxiality implies a difference in the refractive indices along the two minor axes of the refractive index ellipsoid: normal to the tilt plane and in the tilt plane, i.e. $n_y - n_x$. We have also established a technique for measurement of electric field-induced birefringence based on a photoelastic modulator, whereby the in-layer birefringence can be measured to accuracies down to $\pm 10^{-5}$ [16]. The in-plane birefringence in the homeotropic cell alignment measures the difference in refractive indices normal to the electric field (i.e. ***c*** director) and along the electric field, i.e. $n_X - n_Y$. The Y axis is the same as the axis y used for biaxiality; the X axis is, however, different from x and lies along the ***c*** director. This technique gives unique signatures for the various phases and thus is an extremely powerful method for identifying these.

In this paper, we establish the signatures of the E–T phase diagram for the various phases in a well studied compound, 12OF1M7, and determine the characteristics of the various uniaxial and biaxial phases. Furthermore we find that the dependence of the birefringence is similar to that of the tilt angle on temperature and show that like the latter, it follows a power law at the SmC*–SmA phase transition with a tricritical behaviour.

2. Experimental

The material used in the study is a nominally pure (*S*)-1-methylheptyl-4-(4′-dodecyloxybiphenyl-4-ylcarbonyloxy)-3-fluorobenzene [(*S*)-12OF1M7] synthesized by Kingston Chemicals, Hull, UK. The chemical structure of the compound is shown in figure 1.

The following phase sequence is observed on cooling the compound in a homeotropic cell: I 103°C SmA* 91.5°C SmC_α* 89.8°C SmC* 81°C SmC_A*(1/2) 79°C SmC_A*(1/3) 75°C SmC_A*(0). The transition temperatures in general are reduced by about 1–2°C compared with those found previously for the *R* enantiomeric isomer [17, 18]. The transition temperatures measured using a homeotropic cell differ compared with the previous ones measured using a homogeneous cell and these reflect the discrepancies in temperatures between the two cell geometries. These may also result from a small change in the enantiomeric purity. This is possibly due to different batches of chiral 2-octanol used in the synthesis.

Free-standing films of (*S*)-12OF1M7 of approximate 50 μm thickness were prepared to fully cover a hole with a diameter of 1.5 mm drilled in a metal plate; this plate was mounted within a hot-stage the temperature of which could be controlled to an accuracy of ± 10 mK. The optical transmittance of the film at an oblique incidence of 20° was measured using a UV/visible near-IR spectrometer (Perkin–Elmer Lambda 900). The electric field-induced birefringence and the optical rotatory power (ORP) were measured using a homeotropic cell of approximately 30 μm thickness. To obtain the homeotropic alignment, the glass plates were coated with silane (a Dow Corning agent) dissolved in distilled water; these silane-coated plates were cured at a temperature of 100°C for about 1 h. Aluminium rods were used as electrodes for the cell; the gap between the electrodes was set at about 120 μm. The cell was heated to a temperature slightly above that of the isotropic phase transition, filled with the sample and mounted in

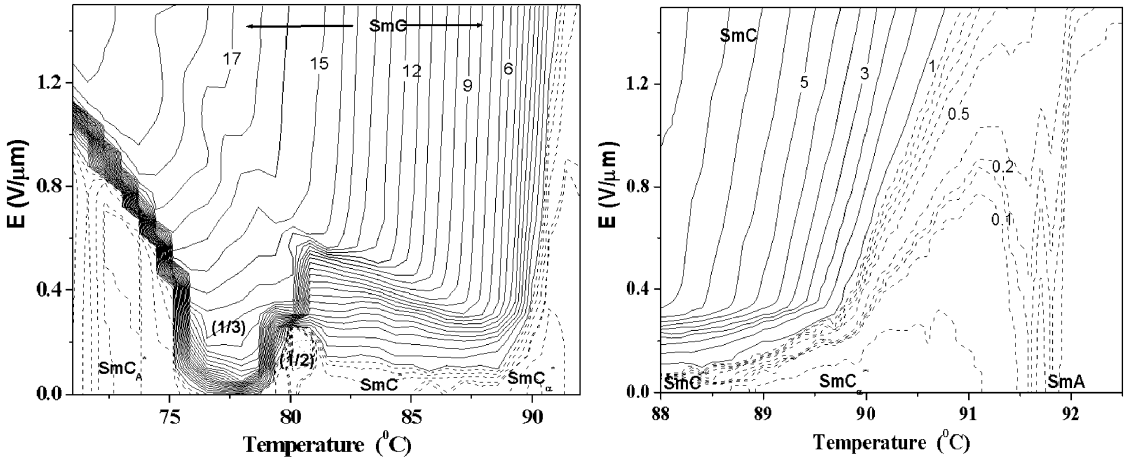

Figure 2. *E–T* phase diagram of the electric field-induced birefringence in a 30 μm thick homeotropic cell of (*S*)-12OF1M7 (a) in the entire temperature range up to SmA phase obtained on cooling at the rate of 0.1°C and (b) in a narrow range of temperatures to show the behaviour in SmC$_\alpha$* and SmA phases. The labels (1/3) and (1/2) represent SmC$_A$*(1/3) and SmC$_A$*(1/2) phases, respectively.

a hot-stage, the temperature of which was controlled to the accuracy specified above. The cell was then cooled slowly to enable SmA phase formation. The homeotropic alignment of the sample was confirmed by visual observations under the polarizing microscope. A He–Ne laser with a wavelength of 632.8 nm and a continuous wave (CW) output power of 2 mW was used as the light source. The ORP was also measured using the same set-up as the birefringence, but after making a slight modification to the hardware [16]. The ORP measurements were made on the cell prior to the application of the electric field. The sample was cooled from its SmA phase down to the relevant temperature in steps of 0.1°C and the ORP data recorded. After this set of measurements, the sample was heated back to the SmA phase and cooled again in steps of 0.1°C and birefringence measurements made at each temperature. The electric field was applied up to 1.5 V μm^{-1} and the electric field-induced birefringence data recorded as a function of increasing field.

Conoscopic observations were also made on homeotropic cells of sample thickness ~200 μm. These cells were prepared in a similar manner to that described above. The gap between the electrodes was set at ~300 μm. The electric field was applied parallel to the substrates. The conoscopic images for the various strengths of the electric field were recorded using a digital video camera (Leica). The *z*-axis was fixed along the long molecular axis, *y*-axis parallel to the direction of the electric field and the *x*-axis (lying in the tilt plane) is perpendicular to both the *z* and *y*-axes. The biaxiality ($n_y - n_x$) was estimated using the method described by Gorecka *et al.* [12].

3. Results and discussion

3.1. *Electric field-induced birefringence*

The electric field-induced birefringence observed for a homeotropic cell of 30 μm sample thickness filled with (*S*)-12OF1M7 is shown in figures 2 a and 2 b. Since the diameter of the spot of the laser beam is slightly larger than that of the gap between the electrodes and, furthermore, the electric field within the area of the spot of the beam is also not uniform, the absolute value of the birefringence may therefore somewhat differ from its true value. The contours of constant birefringence are drawn by solid lines in steps of $\Delta n = 0.7 \times 10^{-3}$ in both figures 2 a and 2 b; some auxiliary contours are shown as dotted lines at steps of 0.1×10^{-3} in the small Δn regions. In figure 2 b, the temperature scale is enlarged and the contours of constant birefringence in both SmC* and SmA phases are shown more clearly. The contour parallel to the electric field axis implies that the birefringence is unaffected by the electric field. However, a set of contour lines of increasing birefringence parallel to the temperature axis implies that the birefringence increases with the electric field. The slanting contours to the temperature axis imply that the birefringence is dependent on both temperature and the electric field. A number of interesting features in this plot are discussed below.

The characteristic pattern in figure 2 b reveals that the SmC$_\alpha$* phase exists over a narrow range of temperatures from 89.8°C to 91.5°C. Figure 2 b clearly shows that the birefringence in the SmC$_\alpha$* phase, although low, is nevertheless much greater than that of the SmA phase. In the SmC$_\alpha$* phase, the contours

show a downward slope of E vs. T, which means that the birefringence increases with the electric field, whereas in the SmA phase the birefringence at zero field is almost zero and with field the contour lines are almost vertical which implies that an increase in birefringence with the field due to the electro-clinic effect is rather negligible. The SmC_α* phase experiences field-induced deformations much greater than those experienced by the SmA phase, especially at temperatures far away from the SmA–SmC_α* transition temperature. The contours of constant birefringence for the SmC_α* phase are different from both the SmA and SmC* phases, allowing for its easy identification.

At zero voltage across the cell, the birefringence shown by the dashed lines is almost zero due to the presence of a helical structure in the cell. As the field increases the birefringence increases, the contours are parallel to the temperature axis. At higher fields the contours become parallel to the electric field axis, which means that the birefringence has almost saturated with the field. The decrease in the slope of the lines indicates that birefringence increases with the field. We note from these contours that the transition from SmC_α* to SmC* is continuous as the lines, from being almost sloping gradually downwards, become vertical as the SmC* phase appears with a decrease in temperature. The phase thus transforms gradually from SmC_α* to SmC* as the temperature decreases and vice versa.

As the sample is cooled down from SmC* phase, we find that the birefringence at a temperature of 81°C drops to almost zero. This shows that a transition to the SmC_A*(1/2) phase has occurred. This phase is exhibited over a temperature range from 79°C to 81°C. First at low electric fields, the birefringence is shown by the dashed curves where the birefringence is very small and mostly negative. The phase is different from SmC* in that in addition to very low values of birefringence at zero electric field, it also exhibits a field threshold. Over a lower narrow range of temperatures from 79–80°C, the phase is seen to transform directly to a ferrielectric phase, before the latter transforms to the SmC* phase, whereas over the higher temperature range of 80–81°C, the reults show that it transforms directly to the SmC* phase. This conclusion is derived from the observations that with an increase in the field, the birefringence contours in the temperature range of 79–80°C become parallel to the temperature axis; the birefringence increases slowly at first and then rapidly with an applied field. Here the phase transforms to a ferrielectric phase (possibly with a three-layer structure). However, for temperatures of 80–81°C, the birefringence first increases with the applied field, saturates and then suddenly starts increasing before again saturating with the field. The threshold at a temperature of 81°C is higher, after which the phase suddenly transforms into the SmC* phase, presumably triggered by the soliton wave [27]. Within the temperature range corresponding to the region separating the two phases with four and three layers, the contours are crowded. The lines are parallel to the electric field. This narrow range of temperatures of 0.3°C width exhibits an interesting behaviour, the details of which will be discussed in a separate publication.

In a narrow temperature range from 79 to 78.5°C, the birefringence contours are crowded. However, within the temperature range 78.5 to 75.7°C, there is a set of birefringence contours parallel to the field, which means that the birefringence increases rather rapidly with applied field, the contours slope upwards and ultimately the contours are almost parallel to the field. This is a normal behaviour for a SmC_A*(1/3) phase where the long macroscopic helical pitch is first unwound, is then converted to a helical distorted SmC* phase and ultimately unwound by increasing the field, giving rise to birefringence contours rather characteristic of this phase.

In the SmC_A*(0) phase, the birefringence is close to zero and it shows a threshold after which the phase is converted to a ferrielectric phase and ultimately to a highly distorted helical SmC* phase, which is finally unwound by increasing the electric field. It is important to note that the threshold for the helical unwinding reflected by a change in the direction of the contours (a step in the ladder) of this two-layer phase is much higher than for the four-layer phase. This is especially interesting in the temperature range that lies in between the phases for two and three layers, where a step ladder of the contours is observed. This step ladder shows that the threshold within the SmC*(0) phase itself varies discreetly rather than continuously with temperature.

To illustrate the different behaviour of the phases, figure 3 shows the dependence of the birefringence on electric field for the four preselected temperatures corresponding to the four different phases: SmC_A*(0), SmC_A*(1/3), SmC_A*(1/2) and SmC*. A comparison between the behaviour of the birefringence in between the two- and four-layer phases shows that, especially in the latter, the birefringence as a function of the electric field turns negative before suddenly increasing rapidly with an increase in the electric field. This shows that in particular, a state is reached where the $\boldsymbol{c}$ directors are aligned in the direction almost parallel to the electric field, i.e. the vertical aligned (VAF) state is achieved even in the four-layer phase [19, 20] where the macroscopic helix is unwound in the pre-transition state before the transition to the ferroelectric state

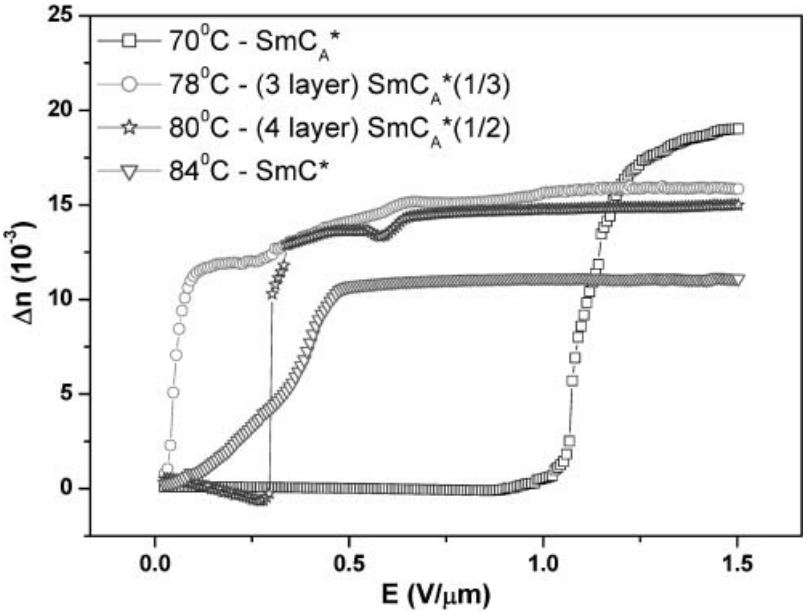

Figure 3. Electric field dependence of field-induced birefringence in different phases: SmC_A*, 70°C; SmC_A*(1/3), 78°C; SmC_A*(1/2), 80°C; SmC*, 84°C.

occurs. This arises from the local polarization of individual layers, as explained by Qian and Taylor [19] and later by Parry-Jones and Elston [20]; however, the resultant or residual polarization of the two- and four-layer phases, as explained by Panarin *et al.* [21], also plays an important role otherwise after an initial threshold voltage the phase should turn directly into SmC*. Thus, if the ***c*** director is directed in the direction of the electric field (Y axis) then the refractive index in the direction normal to it (X axis) is small and therefore the birefringence ($n_X - n_Y$) decreases with an increase in the field as more of the **c** directors are directed towards the electric field. Once this phase is converted into a field-induced ferrielectric or a distorted helical SmC* phase, the macroscopic polarization, P_s, which arises is then directed along the electric field with the **c** director now normal to it, the birefringence increases with an increase in the field and the helix is unwound rather suddenly with a slight additional increase in the field. The critical field for converting a four-layer phase into a field-induced SmC* phase is much lower than that for a two-layer phase, a consequence of their relative stabilities. This leads to the conclusion that the free energy of a two-layer phase is much lower than that of its four-layer counterpart. Another difference between the two- and four- layer phases, as already discussed, is that whereas the latter in general may go directly to an induced SmC* phase, the two-layer phase inevitably passes through a three-layer one since the slope of an increase in the birefringence of the two-layer phase is rather similar to that of a three-layer phase.

Another interesting aspect of the observations is that the maximum field-induced birefringence (figure 4) is found to be dependent on temperature. A higher maximum field-induced birefringence is observed at lower temperatures. This can easily be explained by the temperature dependence of the tilt angle. The higher the tilt angle θ, then higher is the difference in the refractive indices in between that along the **c** director (the length of the c director is proportional to $\sin\theta$) and the direction normal to it, both lying in the smectic layer plane. The results for maximum birefringence as a function of temperature can be fitted by the power law

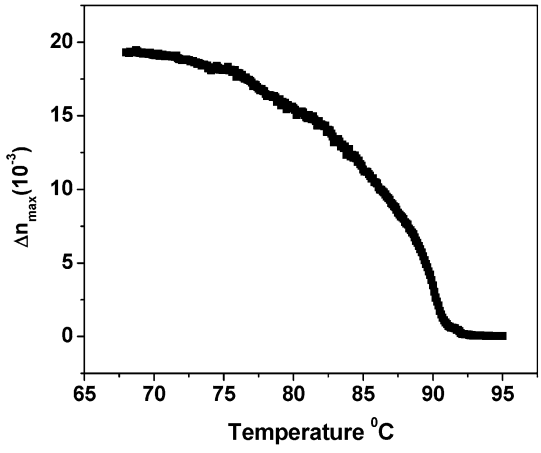

Figure 4. Plot of the maximum in-layer birefringence as a function of temperature.

equation, $(\Delta n)_{\max} = C_1(T - T_0)^{y_1}$ with $C_1 = 6.9 \times 10^{-3}$, $T_0 = 92.01^{\circ}$C and $y_1 = 0.274$.

The exponent y_1 is rather close to 0.25, the value expected from the tricritical point of the phase diagram [22], reflecting a second-order transition from the field-induced SmC* to SmA phase.

From the E–T phase diagrams, it can clearly be seen that the birefringence contours for a perfectly unwound SmC* phase are almost parallel to the field axis (figure 2 a) compared to that in SmA phase where the birefringence contours are oblique (figure 2 b). This indicates that the electroclinic effect is negligible in completely unwound SmC* where the tilt angle is determined mainly by the temperature and independent of the electric field, whereas a large electroclinic effect is observed in the SmA phase. The SmC_A*(1/3) phase is a ferrielectric phase with a net spontaneous polarization which appears under a weak electric field and it has a very long helical pitch that tends towards infinity. This leads to a large birefringence in SmC_A*(1/3) phase, even at very low to moderate electric fields, as clearly seen in figure 3. The completely unwound non-planar structure of the SmC_A*(1/3) phase, which has a three-layer smectic periodicity, stays unwound, as shown by the plateau in figure 3, followed by a further increase in the birefringence with a change to the field-induced distorted SmC*, which is ultimately unwound. The SmC_A*(1/2) phase is distinguishable from SmC_A*(0) phase since the former requires a lower threshold with a comparatively lower critical field for the unwinding process than the latter.

3.2. *The optical rotatory power and birefringence at zero field*

The optical rotatory power (ORP) and the birefringence measured both at zero field give valuable information for the characterization of the phases. For both sets of measurements, the sample is homeotropically aligned and is ~30 μm thick. The measurements, performed during cooling, are shown in figure 5. The set-up for these two cases is a slight modification of each other. The experiments were carried out in sequence to each other prior to the application of the electric field. The SmA phase is optically uniaxial, as already discussed. The SmC_α* phase is also optically uniaxial on the scale of the optical wavelength [7]. Hence, both the ORP and the residual in-plane birefringence for these phases are almost zero in the absence of an applied field. A small birefringence at zero field in the SmC* phase is due to the presence of some domains that may have been partially unwound due to the presence of defects. On cooling the sample, the ORP becomes large in the SmC_A*(1/2) phase and it first changes its handedness

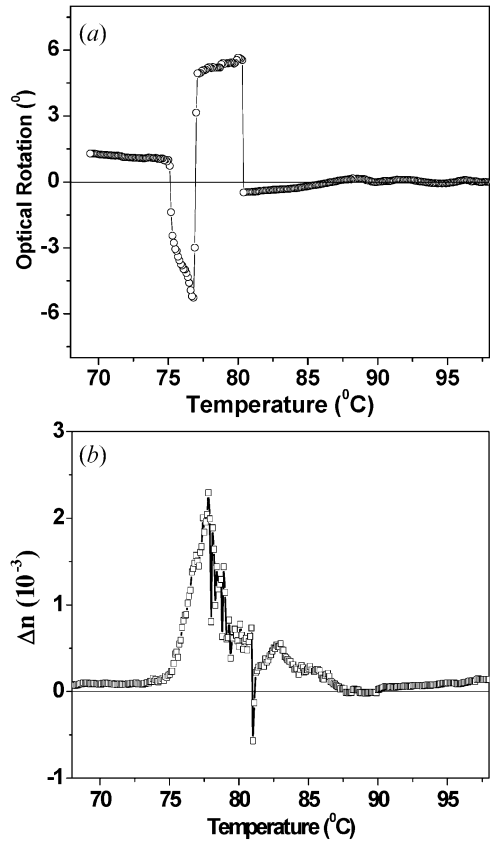

Figure 5. The temperature variation of (a) optical rotatory power and (b) the reduced birefringence measured using a homeotropic cell of 30 μm thickness.

sign on its entry from SmC* phase at 80.5°C. A large birefringence emerges in the SmC_A*(1/3) phase and it remains large. However, before the sample goes into the two-layer phase, the sign of the ORP changes, reflecting a change in the handedness of the helix. The interesting aspect is that this handedness changes within the three-layer phase itself and not at the transition temperature between the two- and three-layer phases. This is feasible due to the presence of a very long helical pitch in the SmC_A*(1/3) phase, where the pitch may diverge to infinity at a certain temperature.

3.3. *Bragg reflection*

The helical structure corresponding to the various smectic phases reflects incident light at some selected wavelengths called Bragg reflections. The dispersion relation for the SmC* phase, studied in detail by Ouchi *et al.* [23], depends on the director's tilt angle and the angle of incidence measured from the helical axis, i.e. the smectic layer normal. The first-order reflection denoted as the full pitch band shows total reflection not only for circularly polarized light but for all planes of

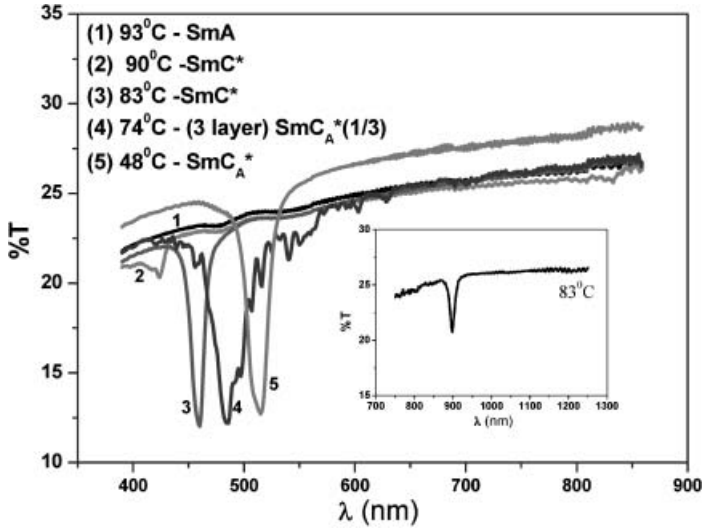

Figure 6. The optical transmittance spectra of free-standing film of (*S*)-12OF1M7 of ~50 μm thickness measured at an angle of oblique incidence of 20° recorded at various temperatures.

polarization, when the light is incident obliquely to the helical axis. It emerges at approximately the wavelength equal to twice the optical helical pitch, (i.e. 2 × mechanical pitch × average refractive index). For normal incidence, there is no reflection from the helical structure and the light penetrates through the cell; the transmitted intensity is almost 100%. The second-order reflection called the characteristic band corresponds to the first-order reflection for a chiral nematic phase. It has a much more complicated dependence on the tilt angle and on the angle of incidence. It is generally a triplet, where a central total reflection band is flanked by the two characteristic reflection bands present on either side of the main band. For normal incidence, however, these three bands coalesce; the central band becomes infinitesimally narrow. The second-order reflection band is circularly polarized. Both the full pitch and the second-order reflection bands are observed in the SmC* phase, but only the latter is observed in the SmC$_A$*(0) and ferrielectric phases. The optical transmittance spectra of a free-standing film of thickness ~50 μm at an angle of oblique incidence of 20° were recorded for various temperatures in the different phases (figure 6). Although we used the same hot stage and the temperature controller, the actual sample temperatures in free-standing films are slightly different from those in a thick homeotropic cell. The spectra (label 3) recorded at 83°C corresponds to the second-order reflection band in the SmC* phase.

In the inset of figure 6, the spectra corresponding to the full pitch band of the SmC* phase at the same temperature is shown at twice the wavelength of the helix. What is very interesting about this material is that helical pitch in SmC* is ~0.3 μm at a temperature close to its transition temperature to SmC$_A$*(1/2) phase. The helix is tightly wound and complexities involved in the helical unwinding process may give rise to complicated dielectric spectra observed over a part of the temperature range of the SmC* phase. It is possible that a tightly wound helix is distorted in a complicated manner by the bias as well as by the weak probe field used in measuring the dielectric spectra; these might have led to this having been identified as a FiLC phase previously, which needs to be investigated.

The characteristic reflection band due to the macroscopic helical pitch in the SmC$_A$*(1/2) phase could not be observed as the pitch is too long and is beyond the window of the experiment. The dips in the transmission spectra at different temperatures measured by the spectrometer correspond to the Bragg reflections, for the first and the second (characteristic reflection band) orders. The helical pitch as a function of temperature can be calculated from the half-pitch reflection band by dividing the wavelength of the selected reflection band by the average refractive index. The selected wavelengths for the bands observed are shown in figure 7. As already shown in figure 6, the transmittance spectra at 74°C, where it borders the two-layer phase, shows multiple dips. Coming from a lower temperature phase, i.e. SmC$_A$*(0), the helical pitch increases significantly even with a further slight increase in the temperature. The multiple reflections at the transition between the two phases arise from the easy deformation of the helical structure of the SmC$_A$*(1/3) phase. Surface effects together with a variation in the number of smectic layers at different places in the film can

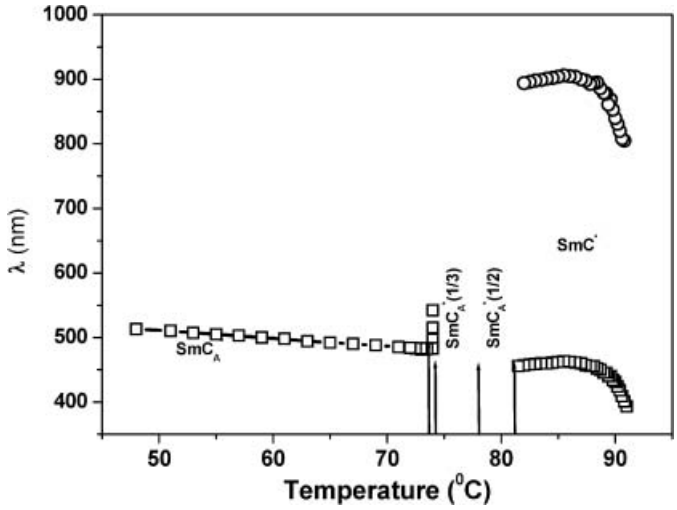

Figure 7. The temperature variation of the half pitch (open squares) and the full pitch (open circles) of (*S*)-12OF1M7 in its various phases.

complicate the half pitch bands in some cases [6]. It has already been shown that the $SmC_A^*(0)$ phase shows a clear characteristic band which turns into a complicated band over a narrow range of temperatures. This was interpreted as an additional phase between the two- and three-layer phases which has later been confirmed to be a five-layer phase [5]. Similar observations have been made here for this enantiomeric compound but are not repeated for the obvious reasons.

The macroscopic helical pitch of the various $SmC^*(q_T)$ phases can be given by [6]

$$\frac{1}{p(\mathrm{SmC_A}^*(q_T))} = -\frac{q_T}{p(\mathrm{SmC}^*)} + \frac{1-q_T}{p(\mathrm{SmC_A}^*(0))}. \quad (1)$$

Equation (1) is based on the assumption that the macroscopic helix of the SmC_A^* phase consists of only A orderings and for the SmC* phase of only F orderings; and the pitch values of the phases are approximately equal but with their handedness opposite to each other. Equation (1) can be used to predict the helical pitch of the phases with different q_T values. Assuming that the helical pitch of the SmC* phase is 0.3 μm and that of $SmC_A^*(0)$ is 0.4 μm, we find that the pitch of the $SmC_A^*(1/3)$ phase is 1 μm and that of the $SmC_A^*(1/2)$ phase turns out to be infinity. These predictions accord well with the observations on this and other compounds.

3.4. *Tilted consoscopy and biaxiality*

Conoscopy is a very powerful technique [12] for investigating biaxial structures. It has successfully been used to discover the structure of antiferroelectric and ferrielectric phases [3]. Conoscopy gives rise to a measurement of the biaxiality and the tilt angle. The biaxiality is defined as the difference in the refractive indices of the two short axes of the refractive index ellipsoid. One of the limitations of the usual conoscopic method is an upper limit of $\sim 18^\circ$ in the tilt angle since the meletopes beyond this angle go out of the field of view. This has been overcome by using a slanted cell and by sandwiching it between prisms made of heavy optical glass. The modified method (called tilted conoscopy) is able to measure the biaxiality of smectic LCs with a tilt angle up to 45° [15]. The conoscopic images recorded for the various sub-phases are shown in figure 8. We could not detect any deviation from the uniaxial behaviour till the sample was cooled down from the isotropic state to SmC* phase. Figure 8 a corresponds to the uniaxial SmA phase, whereas figure 8 b corresponds to the biaxial SmC* phase only when the voltage is applied across the cell. It can clearly be seen from figure 8 b that the uniaxial image due to a helical structure at $E=0$ V changes into a biaxial profile at $E=660\,\mathrm{V\,mm^{-1}}$. In the SmC* phase, the biaxial split occurs in the direction perpendicular to the applied field, indicating that the axis of the minimum refractive index is normal to both the directions of the field and the long molecular axis. As the sample is cooled, the field of view becomes blurred in the $SmC_A^*(1/2)$ phase and a clear conoscopic image cannot be observed and is not shown here. As discussed earlier, the surfaces or a low field strength of the order of a few $\mathrm{V\,mm^{-1}}$ (classified as a low field here) can cause a deformation in $SmC_A^*(1/3)$ phase. In figure 8 c the biaxial profile at $E=40\,\mathrm{V\,mm^{-1}}$ is shown where the biaxial split is now in the direction parallel to the applied electric field, implying that the minimum

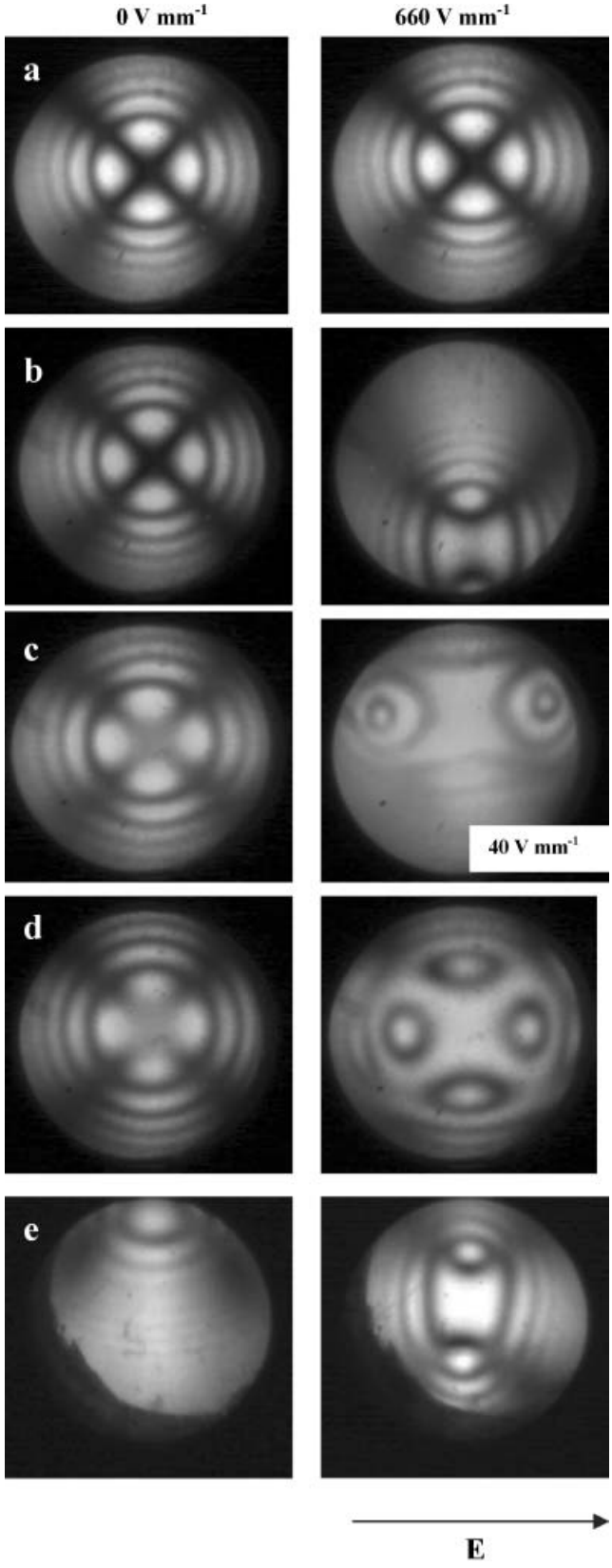

Figure 8. Conoscopic images recorded of the (a) SmA, (b) SmC*, (c) SmC_A*(1/3) and (d) SmC_A* phases, and (e) of the SmC* phase using tilted conoscopy. The applied field, $E=660\,V\,mm^{-1}$ except where indicated, is indicated by the arrow.

refractive index of the ellipsoid is directed along the electric field. In the SmC_A* phase (figure 8 d) no central shift in the conoscopic image at $E=660\,V\,mm^{-1}$ can be observed. The deformation of the conoscopic image on application of the field (figure 8 d) is caused by the local polarization of individual layers, the direction of which alternates from layer to layer. The molecular reorientation was first believed to arise from the dielectric anisotropy interaction [12] but its effect has been found to be negligible.

By cooling the sample to lower temperatures in the SmC* phase, the tilt angle of the material becomes larger and as the angle exceeds $\sim 18^\circ$ the conoscopic image with the usual set-up goes out of the field of view. The method of tilted conoscopy [15] is used to overcome this difficulty. The conoscopic image recorded in the SmC* phase at 88°C using tilted conoscopy is shown in figure 8 e; only a part of the conoscopic picture can be viewed in the absence of the field and for lower tilt angle the technique without tilted cell has to be used. The biaxiality $(n_y - n_x)$ and the apparent tilt angle in SmC* phase are estimated using a standard method given by Gorecka *et al.* [12].

In figure 9, both the apparent tilt angle and the biaxiality in the SmC* phase calculated from conoscopic images at a temperature of 88°C are plotted as a function of the applied voltage. At the field strength where a drastic change in biaxiality occurs, a sudden change in the tilt angle also takes place (figure 9). The field strength at which this change takes place corresponds to the critical field for the unwinding of the helix. Here the helix is not yet completely unwound. An increase in the biaxiality arises from fractures in the helix and the biaxiality reflects the distribution of the ***c*** directors [24]. When the field is increased beyond the critical field, the biaxiality decreases abruptly, which reflects an unwinding of the helix after the helix has been fractured. For larger field strengths, both the tilt angle and the biaxiality saturate and remain almost constant. The saturated values correspond to the local biaxiality and tilt angle at any given temperature.

In figure 10, the estimated local biaxiality and the apparent tilt angle in the SmC* phase are both plotted as a function of temperature. The biaxiality follows the power law equation $n_y - n_x = C_2(T_0 - T)^{y_2}$ with $C_2=0.00071$, $T_0=90.22$ and $y_2=0.54$.

The biaxiality is lower than the birefringence by a factor of almost 10. The tilt angle can be fitted to the power law equation $\theta = C_3(T_0 - T)^{y_3}$ with $C_3=13.656$,

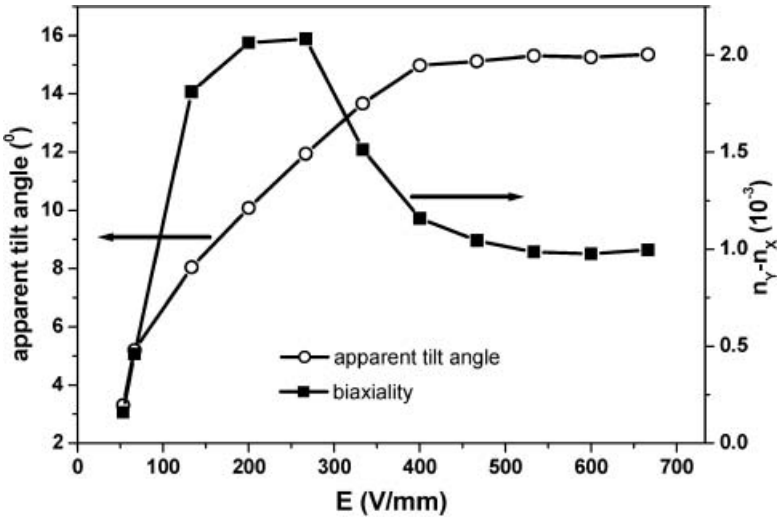

Figure 9. Electric field dependence of biaxiality and the apparent tilt angle of the SmC* phase at 88°C.

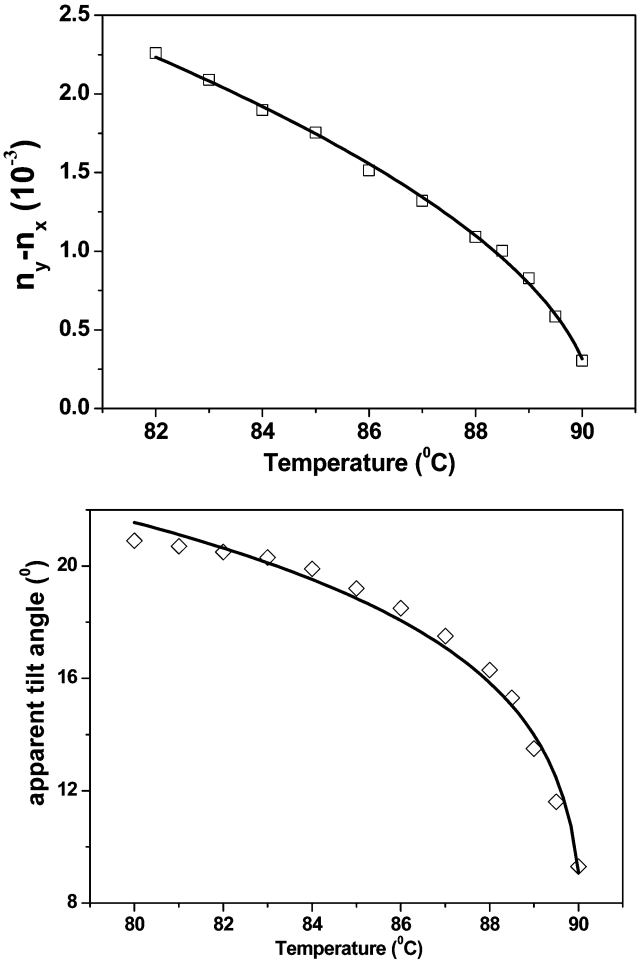

Figure 10. Temperature variation of (a) biaxiality and (b) the apparent tilt angle of (*S*)-12OF1M7 estimated using the conoscopic images of a homeotropic cell of 200 µm thickness.

T_0=90.126 and y_3=0.197. The main point of the fitting is that the exponent for both the tilt angle and the in-plane birefringence is approximately 0.2 and 0.25, respectively, which reflects the tricritical behaviour [22] of the SmC*–SmA phase transition. The exponent for the biaxiality however is approximately equal to 0.5 and it is not known why its value is much higher than for the other parameters. Furthermore, the biaxiality is positive, which suggests that the most polarizable short axis of the molecules is along the direction of the electric field, i.e. the phenyl rings are normal to the tilt plane. The estimated biaxiality reaches a maximum value of $\sim 2.3 \times 10^{-3}$ down by a factor of 10 than the birefringence.

4. Conclusions

The signatures of the electric field-induced birefringence for the various phases of an antiferroelectric liquid crystal have been established. A continuous phase transition from SmC_α* to SmC* is observed. Going from SmC* to SmC_α*, the helical pitch decreases slowly, whereas the slope of the *E*–*T* birefringence plots also changes gradually from one to the other phase with an increase in temperature. A definite characteristic signature for the electric field-induced birefringence for the SmC_α* phase, different from those of the SmC* and SmA phases, is established. The dependence of the birefringence on temperature for the SmC*–SmA transition shows a tricritical behaviour characteristic of a second-order phase transition. The optical transmittance measurements carried out on free-standing films show Bragg reflections for both ferroelectric SmC* and antiferroelectric SmC_A* phases at oblique incidence. A characteristic reflection band with many

dips above the SmC_A* phase is observed. These modulations arise due to fact that the pitch is long and beyond the window of the experiment and clear bands cannot be observed, whereas the modulated structure reflects an easy deformation of this phase by the surfaces. We find that the handedness first changes sign when we go from SmC* to SmC_A*(1/2). We also find that prior to the sample going into a two-layer phase from the high temperature side, the sign of the ORP changes, reflecting a change in the handedness of the helix again. The important finding is that this handedness changes within the temperature range of the three-layer phase itself and not at the transition temperature. This is feasible due to the presence of a very long helical pitch in the SmC_A*(1/3) phase where the pitch can easily diverge and may lead to this result. Birefringence measurements at zero field support this finding as the birefringence during a change in the handedness corresponds to SmC_A*(1/3). Tilted conoscopic measurements carried out on thick homeotropic cells show that the compound (*S*)-12OF1M7 exhibits positive biaxiality throughout the ferroelectric SmC* phase, both during the helical unwinding and even after the helix is completely unwound. The positive biaxiality implies that the fluctuations out of the tilt plane are much greater than those in it and this is what is normally expected of a ferroelectric compound [25]. This also means that, on average, the phenyl rings are normal to the glass plates. The free energy of a two-layer antiferroelectric phase is found to be lower than that of its counterpart four-layer phase. The relative stability and the free energy of these phases determine the phase sequence, in agreement with theoretical predictions [26], by including the various factors that govern the interlayer interactions.

Acknowledgements

We thank the Science Foundation of Ireland (SFI) grant (02/IN.1/I031) for funding research work in Dublin. We thank J. K. Song for the discussions.

References

[1] A.D.L. Chandani, Y. Ouchi, H. Takezoe, A. Fukuda, K. Terashima, K. Furukawa, A. Kishi. *Jap. J. appl. Phys. Pt. 2*, **28**, L1261 (1989).
[2] A.D.L. Chandani, E. Gorecka, Y. Ouchi, H. Takezoe, A. Fukuda. *Jap. J. appl. Phys. Pt. 2*, **28**, L1265 (1989).
[3] A. Fukuda, Y. Takanishi, T. Isozaki, K. Ishikawa, H. Takezoe. *J. Mater. Chem.*, **4**, 997 (1994).
[4] R.B. Meyer, L. Liebert, L. Strzelecki, P. Keller. *J. Phys., Paris*, **36**, L69 (1975).
[5] A.D.L. Chandani, N.M. Shtykov, V.P. Panov, A.V. Emelyanenko, A. Fukuda, J.K. Vij. *Phys. Rev. E*, **72**, 041705 (2005).
[6] V.P. Panov, N.M. Shtykov, A. Fukuda, J.K. Vij, Y. Suzuki, R.A. Lewis, M. Hird, J.W. Goodby. *Phys. Rev. E*, **69**, 060701(R) (2004).
[7] V.P. Panov, B.K. McCoy, Z.Q. Liu, J.K. Vij, J.W. Goodby, C.C. Huang. *Phys. Rev. E*, **73**, 051702 (2006).
[8] K. Hiraoka, Y. Takanishi, K. Skarp, H. Takezoe, A. Fukuda. *Jap. J. appl. Phys. Pt. 2*, **30**, L1819 (1991).
[9] M.A. Osipov, A. Fukuda. *Phys. Rev. E*, **62**, 3724 (2000).
[10] A.V. Emelyanenko, M.A. Osipov. *Phys. Rev. E*, **68**, 051703 (2003).
[11] T. Isozaki, T. Fujikawa, H. Takezoe, A. Fukuda, T. Hagiwara, Y. Suzuki, I. Kawamura. *Jap. J. appl. Phys. Pt. 2*, **31**, L1435 (1992).
[12] E. Gorecka, A.D.L. Chandani, Y. Ouchi, H. Takezoe, A. Fukuda. *Jap. J. appl. Phys. Pt. 2*, **31**, L1435 (1990).
[13] P. Mach, R. Pindak, A.M. Levelut, P. Barois, H.T. Nguyen, C.C. Huang, L. Furenlid. *Phys. Rev. Lett.*, **81**, 1015 (1998).
[14] P.M. Johnson, D.A. Olson, S. Pankratz, H.T. Nguyen, J.W. Goodby, M. Hird, C.C. Huang. *Phys. Rev. Lett.*, **84**, 4870 (2000).
[15] J.K. Song, A.D.L. Chandani, A. Fukuda, J.K. Vij, V. Goertz, J.W. Goodby. *Ferroelectrics*, **344**, 41 (2006).
[16] N.M. Shtykov, A.D.L. Chandani, A.V. Emeylyanenko, A. Fukuda, J.K. Vij. *Phys. Rev. E*, **71**, 021711 (2005).
[17] Y.P. Panarin, O.E. Kalinovskaya, J.K. Vij, J.W. Goodby. *Phys. Rev. E*, **55**, 4345 (1997).
[18] A.A. Sigarev, J.K. Vij, R.A. Lewis, M. Hird, J.W. Goodby. *Phys. Rev. E*, **68**, 031707 (2003).
[19] T. Qian, P.L. Taylor. *Phys. Rev. E*, **60**, 2978 (1999).
[20] L.A. Parry-Jones, S.J. Elston. *Phys. Rev. E*, **63**, 050701(R) (2001).
[21] Yu.P. Panarin, O.E. Kalinovskaya, J.K. Vij. *Liq. Cryst.*, **25**, 241 (1998).
[22] P.G. de Gennes, J. Prost. *The Physics of Liquid Crystals* second edn, Clarendon Press, Oxford (1993).
[23] Y. Ouchi, T. Shingu, H. Takezoe, A. Fukuda, E. Kuze, M. Koga, N. Goto. *Jap. J. appl. Phys.*, **23**, L660 (1984).
[24] S.I. Suwa, Y. Takanishi, H. Hoshi, K. Ishikawa, H. Takezoe. *Liq. Cryst.*, **30**, 499 (2003).
[25] J.K. Song, J.K. Vij, I. Kobayashi. *Phys. Rev. E*, **75**, 051705 (2007).
[26] A.V. Emelyanenko, A. Fukuda, J.K. Vij. *Phys. Rev. E*, **74**, 011705 (2006).
[27] J.K. Song, A. Fukuda, J.K. Vij. *Phys. Rev. E*, **76**, 011708 (2007).